J. Electrochem. Sci. Eng. **15(2)** (2025) 2618; http://dx.doi.org/10.5599/jese.2618

Open Access : : ISSN 1847-9286
www.jESE-online.org

Original scientific paper

Pyrazolone derivatives as corrosion inhibitors of copper in sulfuric acid solution

Rehab E. Azooz[1,✉], Salah M. Abd El-Haleem[2] and Ahmed Diab[2]

[1]*Department of Physical Sciences, Chemistry Division, College of Science, Jazan University, P.O. Box. 114, Jazan 45142, Kingdom of Saudi Arabia*

[2]*Chemistry Department, Faculty of Science, Zagazig University, Zagazig, Egypt*

Corresponding author: ✉ *rramadan@jazanu.edu.sa; Tel.: +966 532324115*

Received: December 27, 2024; Accepted: February 5, 2025; Published: February 14, 2025

Abstract

This study examines the corrosion inhibition of copper in aerated H_2SO_4 solution using 5-methyl, 5-phenyl, and 5-methyl-2-phenyl derivatives of 2,4-dihydro-3H-pyrazol-3-one (Py) through electrochemical techniques, gravimetric method, SEM, DFT and Monte Carlo simulation. The results showed that these compounds exhibited good inhibition efficiency, increasing in the order: Py II (84.9 %) < Py III (87.9 %) < Py I (90.1 %) at 10 mM. The protection efficiency improved with higher inhibitor concentration and decreased with rising temperature. Thermodynamic parameters for the inhibition process were calculated, with ΔH_{ads}^0 values of -17.76±0.607, -15.8±0.101 and -16.24±0.118 kJ mol^{-1} for Py I, Py II and Py III, respectively, confirming the exothermic nature of adsorption. The adsorption followed the Langmuir isotherm and occurred physically and spontaneously. Monte Carlo simulations indicated that PYs adsorbed in a parallel configuration, provide better coverage of the metal surface with high adsorption energy. SEM confirmed formation of a protective layer. Based on experimental and theoretical data, pyrazolone derivatives are recommended as corrosion inhibitors for copper in H_2SO_4 media.

Keywords

Metal corrosion; pyrazole compounds; inhibition efficiency; adsorption isotherm; DFT calculations; molecular dynamics simulations

Introduction

Owing to its favorable properties like high electrical and thermal conductivity, mechanical workability, malleability and resistance to atmospheric and chemical agents, copper is used in a wide range of industrial applications [1,2]. One of the most important applications of copper are industrial applications equipment, marine industry, power stations, coinages, electricity and desalination plants, heat exchanges and cooling power [3,4]. Despite its relatively noble character, copper dissolves in severe industrial environments like oxidizing acids *e.g.* HNO_3 and H_2SO_4. It also dissolves in acidic environments containing chloride, sulphates and nitrates [5,6] .

Because it is a stronger acid, generally more stable and safer to handle in a variety of industrial processes, sulfuric acid (H_2SO_4) is frequently used in corrosion studies instead of hydrochloric acid (HCl). It also has a higher degree of ionization, which can be helpful in reactions that require a strong acidic environment, and strong dehydrating properties that make it useful in reactions where water removal is crucial. Because it is less volatile than hydrochloric acid, which reduces the likelihood of hazardous vapors, it is a more versatile choice. It is also widely used in a variety of applications, including the production of detergents, dyes, and fertilizers.

As a result of the widespread use of copper within industrial acidic media, several studies were carried out using organic and inorganic materials as copper-based inhibitors. Aromatic compounds like amines and their derivatives containing a nitrogen atom that facilitates their adsorption on the metal surface and the formation of a protective barrier have been used extensively as organic corrosion inhibitors in acidic media [7]. Additionally, several investigations using organic compounds with 5-membered rings containing heteroatoms like oxygen, nitrogen, and sulfur were used to inhibit copper corrosion [8]. Copper corrosion has been observed to be inhibited in acidic environments by azoles and related derivatives. These compounds exhibit a remarkable inhibition efficiency due to their abundant donor atoms. The adsorption of these compounds frequently follows the Langmuir isotherm [9].

Pyrazole compounds are non-toxic, inexpensive and considered as a green and environmentally friendly inhibitor. They include functional groups like N, O, and pyrazolone rings. Their inhibitory action for copper and mild steel was explained using a range of methodologies, including electrochemical methods and weight loss assessments [10]. The mode of action of these compounds depends on their adsorption onto the metal surface. Lgaz *et al.* [11,12] used pyrazoline derivatives to inhibit mild steel corrosion in HCl solution. These compounds behave as mixed-type inhibitors and their adsorption obeys the Langmuir adsorption isotherm. On the other hand, Chaouiki *et al.* [13], used 2-(4-(3-phenyl-4,5-dihydro-1Hpyrazol-5-yl)phenoxy) acetic acid to inhibit the corrosion of mild steel in HCl solution using various techniques. The experimental results revealed that the studied compound gave a maximum inhibition efficiency of 87 % and the inhibition ability increased with raising of the inhibitor concentration. Computational calculations such as density functional theory (DFT) and molecular dynamic (MD) simulations correlate well with electrochemical parameters obtained.

The present investigation is concerned with the use of some pyrazolone derivatives as corrosion inhibitors for copper corrosion in H_2SO_4 using polarization and gravimetric methods. The investigation focused on the impact of inhibitor concentration, temperature, and duration immersion on the corrosion rate. The thermodynamic parameters associated with the inhibition process were computed. MD and DFT studies were performed to follow the adsorption configuration, adsorption energy, and quantum chemical descriptors. Upon integration of the experiment findings, the molecular-level mechanism of inhibitors surface adsorption could be elucidated, together with critical variables influencing the inhibitory performance.

Experimental

Experiments were carried out on copper sheets and/or rods with the following composition: 0.027 wt.% Ni, 0.067 wt.% Zn, 0.006 wt.% Se, and the remainder Cu 99.90 wt.%.

Solutions

Electrolyte solutions were prepared using analytical grade reagents and triple distilled water. H_2SO_4 solutions (BHD grade) with completely different concentrations were prepared. Figure 1

displays chemical configurations of the pyrazolone derivatives. The concentration range of the pyrazolone compounds (inhibitors) (Analytical grade purchased from Al-Gomhoria Company, Egypt and have high solubility in acidic medium) used was between 0.1 and 10 mM. The measurements were validated at 25±0.1 °C. The cell temperature was controlled with an ultra-thermostat from Polyscience (USA).

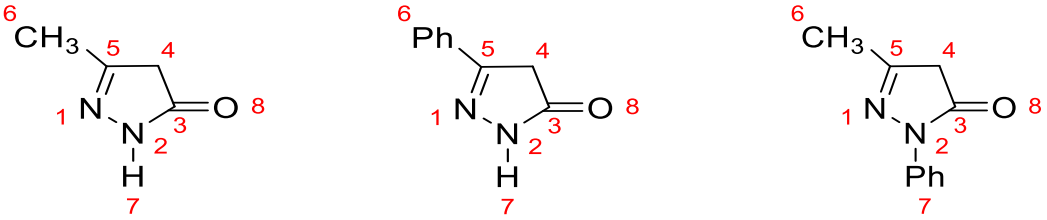

Figure 1. *Chemical configurations of pyrazolone derivatives*

Weight loss measurements

Five parallel copper sheets measuring 5.0×2.0×0.2 cm were abraded with emery paper (grades 320–500–800) and then washed with demineralized water and dried with acetone After accurate weighing, the specimens were completely buried in a beaker containing 250 ml of the tested solution (sulfuric acid) without or with pyrazolone derivatives in varying concentrations. Following the appropriate immersion period, the specimens were pulled out, cleaned, dried, and precisely weighed. The average weight loss of five parallel copper sheets was obtained. The inhibitory efficiency (IE) and the surface coverage (θ) of pyrazolone compounds for the copper inhibition were calculated (equation 1) as follows [10] :

$$IE = 100\ \theta = 100\ (W^0\text{-}W)/W^0 \quad (1)$$

where W^0 and W stand for the average weight loss for the free acid solution and in the presence of pyrazolone compounds, respectively.

Polarization measurements

In this section, testing was carried out in a cell with three openings: one for a standard reference electrode (SCE), one for a Pt counter electrode, and one for the working electrode. Using epoxy adhesive, the working electrode, a 0.350 cm diameter copper rod was inserted into a salt glass pipe, revealing 0.785 cm². A dense copper wire attached to the copper bar that was not in touch with the solution was used to create electrical connections. Using a Jean Wirtz TG 200 grinding machine, the metal conductor was consistently surface-prepared with successive 0-, 00-, and 000-grade sandpaper papers before use. It was then flushed with a solvent, cleaned with distilled water, and submerged in the solution.

The scanning rate used for all potentiodynamic polarization tests was 5 mV s^{-1}. By extrapolating the anodic and cathodic Tafel lines to obtain log i_{corr} the Stern-Geary method was utilized to quantify the corrosion current (i_{corr}) and the related corrosion potential (E_{corr}) for the tested solutions. The inhibition efficiency (IE) and surface coverage (θ) were then determined using the corrosion current density (i_{corr}) , as shown by Equation 2 [10]:

$$IE = \left[1 - \frac{i_{corr(inh)}}{i_{corr(free)}}\right] 100 = 100\,\theta \quad (2)$$

where, $i_{corr\ (free)}$ and $i_{corr(inh)}$ are corrosion current densities without and with pyrazolone compound solutions, respectively.

Computational study

Optimizing geometry for pyrazolone derivatives

All used pyrazolones were drawn using Chem-Draw 19.1 as portrayed in Figure 1, then uploaded to Gaussian 09, using density functional theory (DFT) based on the 6-31G basis set and B3LYP method as the level of theory to calculate energetic behavior and quantitative chemical descriptors. The most used quantum mechanical molecular descriptors include the highest occupied molecular orbital energy (E_{HOMO}) lowest unoccupied molecular orbital energy (E_{LUMO}), energy gap (E_{gap}), ionization potential (I), electron affinity (A), global hardness (η), global softness (σ) , absolute electrophilicity index (ω), global electronegativity (χ) and dipole moment (μ). Where E_{gap}, I and A were calculated from E_{HOMO} and E_{LUMO} values using the Equations (3(to-(5) [11]:

$E_{gap} = E_{LUMO} - E_{HOMO}$ (3)

$I = - E_{HOMO}$ (4)

$A = - E_{LUMO}$ (5)

Both I and A values are exploited to obtain χ and η of the inhibitory molecule [14] from Equations (6 and 7):

$$\chi = \frac{1}{2}(I + A) = \frac{1}{2}(E_{LUMO} + E_{HOMO}) \quad (6)$$

$$\eta = \frac{1}{2}(I - A) = \frac{1}{2}(E_{LUMO} - E_{HOMO}) \quad (7)$$

To compute the transferred fraction of electrons (ΔN), equation (8) [14], It is assumed that Cu_{bulk} atoms are softer than neutral Cu atoms, with a value of 4.48 eV/mol [15]. Additionally η_{Cu} is assumed to be 0 eV/mol. Considering that for a Cu_{bulk}, $I = A$ [16]. Equation (8) can be expressed as follows

$$\Delta N = \frac{1}{2}\left(\frac{\chi_{Cu} - \chi_{inh}}{\eta_{Cu} + \eta_{inh}}\right) \quad (8)$$

The formulas for the calculation of several descriptors mentioned are given by Equations (9) and (10) [17]:

$$\sigma = \frac{1}{\eta} \quad (9)$$

$$\omega = \frac{\chi^2}{2\eta} \quad (10)$$

The optimization process using the DMol3 module in BIOVIA Material Studio software was employed to determine the condensed Fukui function. This function is identified as the first derivative of electron density, $\rho(r)$, in proportion to the number of electrons, N, at a fixed external potential $\nu(r)$, which illustrates how a molecule changes electron density at a specific position as the counts of electrons vary [18,19]. Fukui indices (f_k^+, f_k^- and f_k^0) are helpful to investigate the molecule responsiveness calculated from equations (11) to (15):

$$f(r) = \frac{\partial \rho(r)}{\partial N}_{\upsilon(r)} \quad (11)$$

$f_k^+ = [r_k(N) - r_k(N\text{-}1)]$ for nucleophilic attack (12)

$f_k^- = [r_k(N+1) - r_k(N)]$ for electrophilic attack (13)

$f_k^0 = 1/2\ [r_k(N+1) - r_k(N\text{-}1)]$ for radical attack (14)

$Df(k) = f_k^+ - f_k^-$ (15)

where for site k, the electronic densities of anionic, neutral, and cationic species are $r_k(N+1)$, $r_k(N)$ and $r_k(N\text{-}1)$ respectively. $Df(k)$ is the dual descriptor, where, its positive and negative signs refer to

electrophilic species and nucleophilic species respectively. Sites with the highest probability of experiencing nucleophilic and electrophilic assaults are verified by the highest values of f_k^+ and f_k^-, respectively [20].

Molecular dynamic simulation

Although each orientation of Cu has unique benefits depending on its intended purpose, $Cu_{(111)}$ is widely utilized because of its stability and beneficial surface properties. Electrical and catalytic characteristics of copper surfaces are often studied, and different crystal orientations exhibit a variety of characteristics. Since $Cu_{(111)}$ is often copper's lowest energy face, its surface characteristics may be more consistent and distinct. Because it is typically more stable and less reactive than $Cu_{(110)}$ and $Cu_{(100)}$ surfaces, it is also less prone to reconstruction or surface flaws. The closely packed $Cu_{(111)}$ surface and its electrical characterization allow for better adsorption of some molecules, which may be useful in corrosion and catalytic processes [21].

Pure $Cu_{(111)}$ was enlarged to supercell to offer an extensive surface for the interaction with each inhibitor. The MD run in a 5×5 supercell featuring the force field of COMPASS, A temporal step of 1 fs, and an imitation period of 500 ps in a container of ($1.28\times1.28\times2.54$ nm^3) in even temperature of 303 K was employed with the Materials studio package.

Results and discussion

Weight-loss measurements

Effect of sulfuric acid concentration

When copper was soaked in a sulfuric acid solution, it became at risk of corrosion. The following equations (18) to (21) can be used to illustrate the different stages of the copper's dissolving reaction in the sulfuric acid solution [22,23]:

$$Cu \rightarrow Cu^{2+} + 2e^- \quad (18)$$

This reaction can be displayed in two steps, each involving one electron:

$$\text{Step 1: } Cu \leftrightarrow Cu^+ + e^- \quad (19)$$

$$\text{Step 2: } Cu^+ \rightarrow Cu^{2+} + e \quad (20)$$

where step 1 lies under equilibrium conditions and step 2 is the slower step in the sequence of the reaction, *i.e.* the copper dissolution is an activation-controlled process. In naturally aerated acid solutions, the rate-determining step during dissolution of copper is oxidation of (Cu^+) [24]:

$$Cu^+ + 2H^+ + 1/2\ O_2 \rightarrow Cu^{2+} + H_2O \quad (21)$$

Equation (21) suggests that copper-anodic dissolution in naturally aerated acid solutions is an activation-controlled process. Gravimetric measurements were performed for copper specimens immersed through 10 to 60 hours of immersion time at 25 °C in different concentrations, ranging from 0.1 to 0.5 M H_2SO_4. The weight loss variation for copper coupons in 250 ml of varying H_2SO_4 concentrations at 25 °C is shown in Figure 2 as a function of immersion time, where straight lines were obtained as results.

Figure 3 displays the plot of the log (weight loss) against the duration of immersion time to track the kinetics of the dissolution reaction of copper species at various sulfuric acid concentrations at 25 °C This figure shows straight-line correlations that indicate a first-order reaction for copper corrosion in sulfuric acid. The first-order rate law (Equation 22) was used to get the values of the rate constant (k) [25].

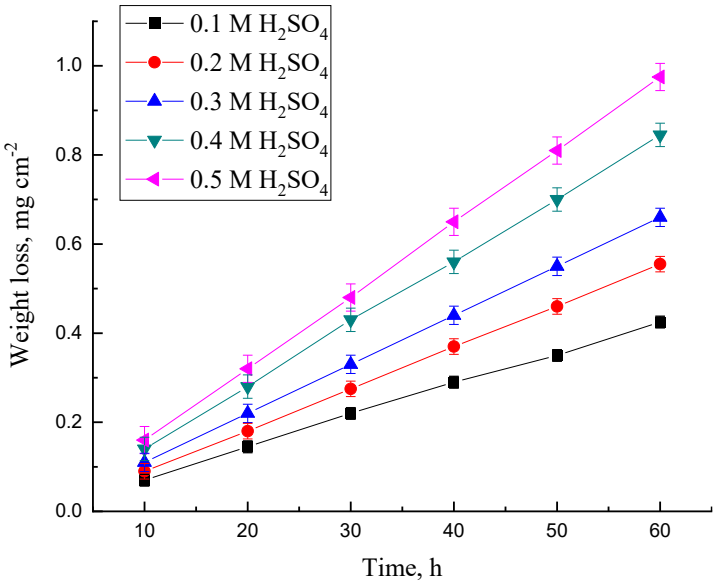

Figure 2. *Variation of weight loss of copper with immersion time in different concentrations of H_2SO_4 solution at 25 °C*

$$k = \frac{2.303}{t} \log W \tag{22}$$

where W is the weight loss of Cu after a period (t). From the parallel straight lines of Figure 3, the values of the slopes were calculated. By substituting these values in Equation (22), the rate constant (k) was calculated to be 3.915x10-3 h^{-1} The half-life ($t_{1/2}$) was obtained by Equation (23) [25]:

$$t_{1/2} = \frac{0.693}{k} \tag{23}$$

Substituting the values of k into Equation (23), half-life time ($t_{1/2}$) for the copper dissolution process was found to be equal to 177 hours.

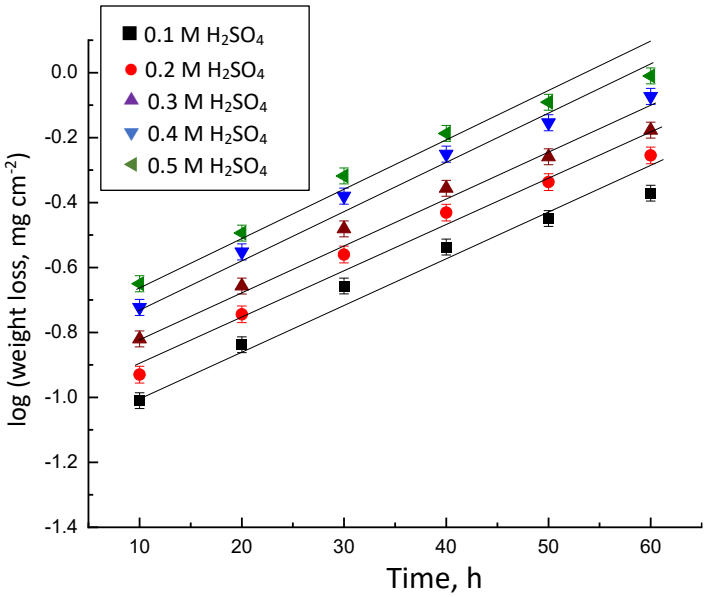

Figure 3. *Log of weight loss versus immersion time for copper in different concentrations of sulfuric acid at 25 °C*

Effect of temperature

The impact of raising the temperature from 25 to 55 °C on the copper corrosion rate in a naturally aerated 0.5 M H_2SO_4 solution is further investigated. The fluctuation of W for copper dissolution in 0.5 M H_2SO_4 solution at varying temperatures is shown in Figure 4 concerning immersion time (t).

The straight lines in Figure 4 demonstrate that as the temperature rises, the rate of corrosion of copper is markedly increased.

The Arrhenius equation (Equation (24)) can be used to express how temperature affects the rate of copper corrosion (r) [10]:

$$\log r = \text{constant} + \frac{\Delta E_a}{2.303RT} \quad (24)$$

where r is the corrosion rate, ΔH_{ads} is the activation energy of the corrosion reaction, T is the absolute temperature, and R is the universal gas constant. The Arrhenius plots for the copper corrosion rate in 0.5 M H_2SO_4 are displayed in Figure 5 (after 10 h of immersion). These findings produce a straight line with the slope from which the activation energy (ΔH_{ads}) can be determined. It was found that ΔH_{ads} equals 12.16 kJ mol^{-1}.

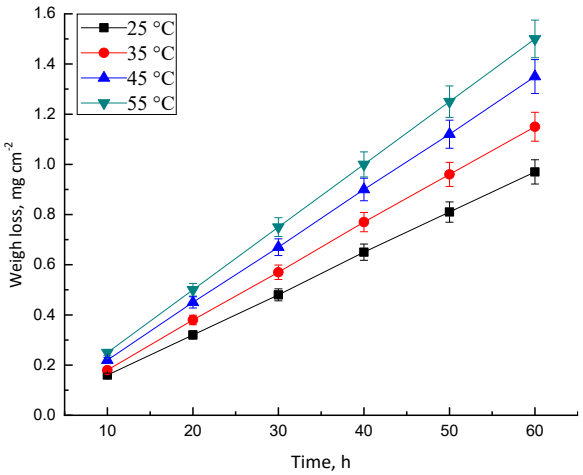

Figure 4. *Variation of weight loss of copper with immersion time in 0.5 M H_2SO_4 at different temperatures*

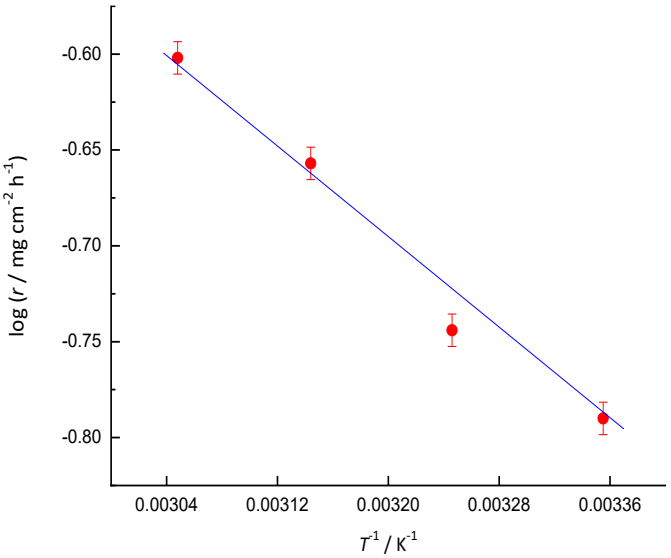

Figure 5. *Arrhenius plot of corrosion rate against T^{-1} for copper in 0.5 M H_2SO_4 after immersion time of 10 h*

Effect of addition of pyrazolone derivatives

In the present part of this work, it was of interest to highlight the effect of some pyrazolone derivatives as inhibitors for the corrosion of copper in 0.5 M H_2SO_4 acid solution. Increasing concentrations of Py I, Py II and Py III were used to inhibit the corrosion of copper in 0.5 M H_2SO_4.Figure 6 represents the variation of weight loss of copper with immersion time in 0.5 M H_2SO_4 at increasing concentrations of Py at 25 °C (similar curves are obtained for other pyrazolone derivatives.).

Inspection of the curves of Figure 6, the values of weight loss of copper was decreased with increasing the concentrations of PY I. The curves of Figure 7 represent the variation of the weight loss of copper with immersion time at adjusted concentration of pyrazolone derivatives as 10 mM in 0.5 M H_2SO_4 at 25 °C.

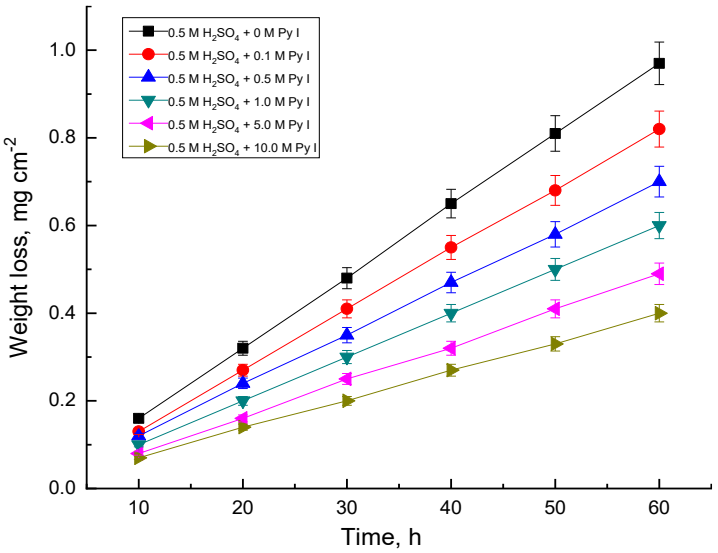

Figure 6. *Variation of weight loss of copper with immersion time in 0.05 M H_2SO_4 without and with increasing concentrations of Py I at 25 °C*

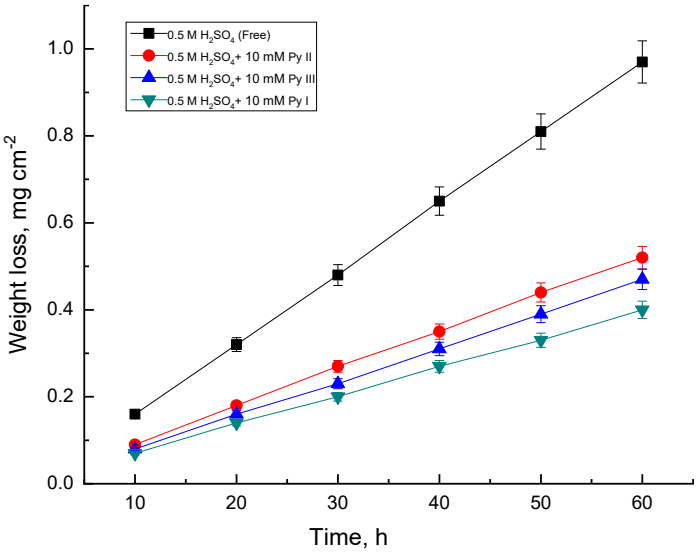

Figure 7. *Variation of weight loss of copper with immersion time at 0.5 M H_2SO_4 without and with 10 mM concentration of three pyrazolone derivatives at 25 °C*

This behavior could be attributed to the inhibiting effects of these compounds which retard the dissolution process and assist the inhibition process. It is clear from the curves of Figure 7 that the lowest values in the loss in weight for copper species dissolution in 0.5M H_2SO_4 occurs in presence of Py I than the other additives. Further inspection of Figure 7 indicates that the inhibition efficiency of these compounds increased in the following order: (low inhibition) Py II < Py III < Py I (high inhibition).

The action of the used pyrazolone additives as corrosion-inhibiting compounds could be detected from the values of the inhibition efficiency (IE) equation (25) for each additive which is defined by the following equation [10]:

$$IE = 1 - (W/W_0)100 \quad (25)$$

where W_o and W are the weight loss in the absence and presence of inhibiting compounds, respectively. The values of IE for the inhibiting compounds used (after 10 hours) can be seen in Table 1, which reveals the following conclusions to be drawn:

- IE of each inhibitor increases with increasing its concentration.
- At the concentration of the same additive, IE increases in the following order: Py II < Py III < Py I

Table 1. *Variation of inhibition efficiencies of copper immersed in 0.5 M H_2SO_4 for 10 hours using various doses of pyrazolone derivatives, at 25°C*

c_{Py} / mM	IE, %		
	PyI	PyII	PyIII
0.1	19	6	13
0.5	25	13	19
1.0	38	25	31
5.0	50	38	44
10.0	57	44	50

Polarization measurements

Potentiodynamic polarization behavior of the copper electrode in 0.1 to 0.5 M sulfuric acid at 25 °C, is illustrated in Figure 8. Inspection of the curves of Figure 8 reveals that on increasing the concentration of H_2SO_4, shifts the anodic polarization curves to a more active direction, while the cathodic polarization curves shift to a more anodic direction.

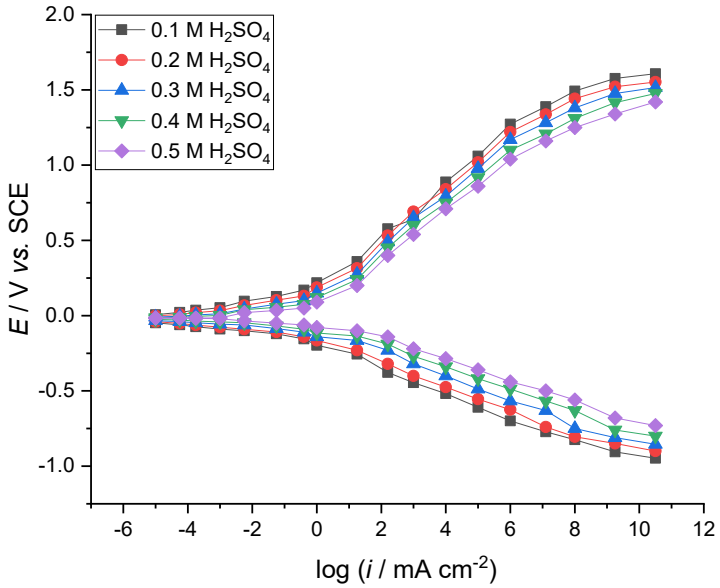

Figure 8. *Potentiodynamic polarization curves of the copper electrode in various concentrations of H_2SO_4 solution at 25 °C and scanning rate 5 mV s^{-1}*

The numerical values of the variation of corrosion current density (i_{corr}), corrosion potential (E_{corr}), and Tafel slopes (β_a and β_c), with the changing sulfuric concentrations are provided in Table 2. The polarization resistance was obtained from the Stern-Geary equation [26] and the corrosion rate of copper was determined from Equation (26) [27]:

$$\text{Corrosion rate} = 0.1288\, i_{corr}\, \frac{w_{eq}}{D} \qquad (26)$$

where w_{eq} = 31.8 is the equivalent weight of metal (working electrode) and D = 8.96 g cm^{-3} is the density of metal. The computed data derived from Figure 8 and Table 2 show that Tafel-type

behavior is shown by the both cathodic and anodic curves. The anodic and cathodic polarization curves change to more active and noble directions, respectively, as the concentrations of H_2SO_4 increase. The values of i_{corr} increase, E_{corr} shifts to more active directions, R decrease, and the rates of corrosion increase. This trend indicates that when the concentration of sulfuric acid solution increases, copper electrode dissolution increased markedly and readily.

Table 2. *Kinetic parameters of Cu electrode in various concentrations of H_2SO_4 solution at 25°C, as calculated from Figure 8 and Equation (26)*

$c_{H_2SO_4}$ / M	Corrosion rate, mm year^{-1}	$-E_{corr}$ /mV *vs.* SCE	I_{corr} / mA cm^{-2}	β_a / mV dec^{-1}	β_c / mV dec^{-1}	R_p / kΩ
0.1	0.005	19.8	0.013	239.3	-146.3	3.032
0.2	0.009	30.7	0.021	227.4	-128.8	1.701
0.3	0.027	36.2	0.062	213.5	-111.4	0.513
0.4	0.091	42.8	0.211	202.6	--88.5	0.138
0.5	0.287	48.6	0.631	194.8	100.3	0.042

Figure 9 shows the impact of adding progressively higher concentrations of Py I (one of the evaluated pyrazolone derivatives) on the electrochemical behavior of copper in 0.5 M H_2SO_4. Table 3 contains the electrochemical characteristics that were determined for the investigated pyrazolone derivatives, including E_{corr}, Tafel slopes (β_c and β_a), corrosion rates, and i_{corr} values.

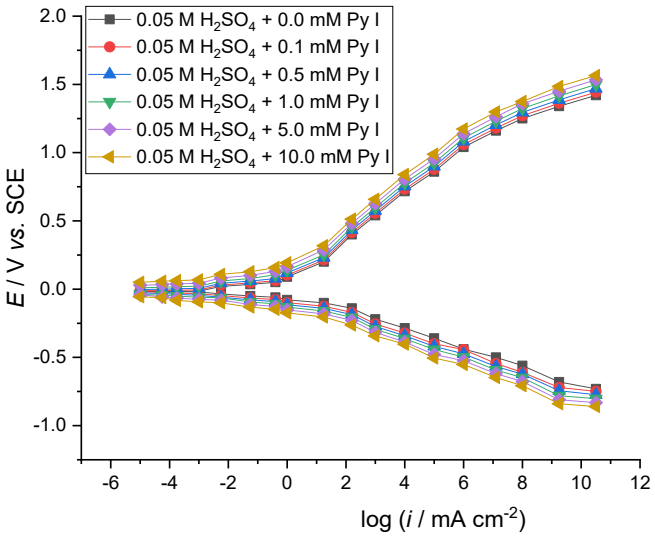

Figure 9. *Potentiodynamic polarization patterns of the copper electrode in 0.5 M H_2SO_4 solution without and with increasing concentrations of Py I at 25 °C and scanning rate 5 mV s^{-1}*

Examining the data in Figure 9 and Table 3 indicates that when the concentration of these additives increases, the corrosion potential (E_{corr}) of copper shifts towards more positive potentials, leading to increased adsorption on the copper surface [28]. The values of the corrosion rates decreased upon increasing the concentrations of added pyrazolone compounds. This behavior demonstrated the high inhibitory activity of these pyrazolones. Figure 10 represents Tafel-plots for copper electrode in 0.5 M H_2SO_4 in the absence and presence of different Py concentrations, the order of increasing IE is: (lower inhibition) Py II < Py III< Py I (higher inhibition). This is in good agreement with the behavior resulting from weight loss measurements and confirms the ability of those inhibitors to reduce corrosion of Cu in 0.5 M H_2SO_4 as compared to other derivatives listed in Table 4.

Table 3. *Kinetic parameters for the inhibition of copper corrosion in 0.5 M H_2SO_4 without and with increasing pyrazolone derivative concentrations at 25 °C and computed using Equation 26 and Figure 10*

c_{Py} / mM	Pyrazolone derivate	Corrosion rate, mm year^{-1}	- E_{corr}/ mV (SCE)	I_{corr}/ mA cm^{-2}	β_a/ mV dec^{-1}	β_c / mV dec^{-1}	R_p / kΩ	θ	IE, %
0.00	-	0.287±0.03	48.6	0.631	194.8	-88.5	0.042	-	-
0.11	Py I	0.181±0.05	36.6	0.398	204.2	-106.2	0.076	0.369	36.9
0.15		0.114±0.05	28.7	0.251	213.8	-119.7	0.133	0.602	60.2
1.00		0.072±0.05	17.4	0.158	227.6	-127.1	0.224	0.749	74.9
5.00		0.046±0.05	11.2	0.102	231.1	-138.5	0.368	0.838	83.8
10.00		0.028±0.05	5.5	0.063	238.7	-143.6	0.617	0.901	90.1
0.11	Py II	0.256±0.07	44.2	0.562	198.3	-92.7	0.049	0.109	10.9
0.15		0.162±0.07	39.8	0.355	207.4	-99.3	0.082	0.469	46.9
1.00		0.102±0.07	33.2	0.224	213.6	-106.4	0.138	0.645	64.5
5.00		0.064±0.07	25.3	0.141	221.8	-117.5	0.237	0.776	77.6
10.00		0.043±0.07	18.7	0.095	225.2	-124.3	0.366	0.849	84.9
0.11	Py III	0.218±0.06	41.3	0.478	199.8	-99.8	0.060	0.242	24.2
0.15		0.138±0.06	34.5	0.302	210.2	-111.2	0.105	0.521	52.1
1.00		0.087±0.06	26.4	0.191	219.5	-121.2	0.178	0.697	69.7
5.00		0.054±0.06	19.2	0.120	226.2	-130.4	0.299	0.809	80.9
10.00		0.036±0.06	10.3	0.079	233.4	-137.5	0.475	0.874	87.4

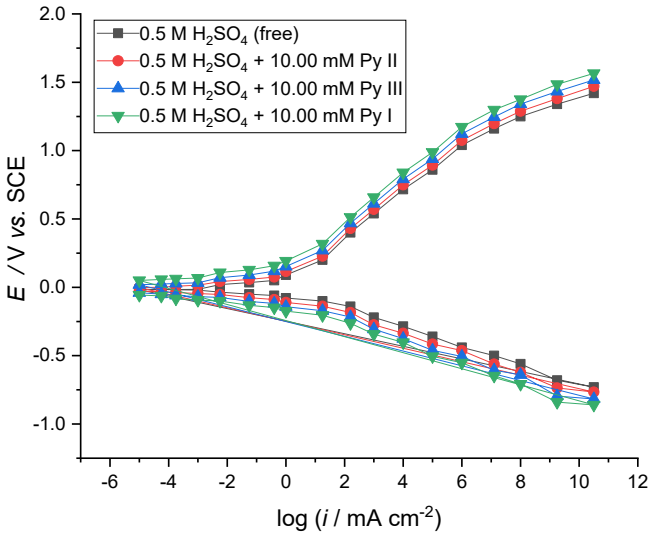

Figure 10. *Potentiodynamic polarization curves of the copper electrode in 0.5 M H_2SO_4 solution without and with 10 mM of pyrazolone derivatives at 25 °C and scanning rate 5 mV s^{-1}*

Table 4. *List of pyrazolone derivatives utilized as corrosion inhibitors for various metals*

Inhibitor	Electrode	Medium	IE %	Adsorption isotherm	Ref.
2-(4-(5-(p-tolyl)-4,5-dihydro-1H-pyrazol-3-yl)phenoxy)acetic acid (P1) and 2-(4-(5-(4-nitrophenyl)-4,5-dihydro-1H-pyrazol-3-yl)phenoxy)acetic acid (P2)	Mild steel	1.0 M HCl	>80	physisorption as well as chemisorption	[11]
2-(4-(4,5-dihydro-3-(4-methoxyphenyl)-1H-pyrazol-5-yl)phenoxy)acetic acid (PYR-1) and 2-(4-(4,5-dihydro-3-p-tolyl-1H-pyrazol-5-yl)phenoxy)acetic acid (PYR-2)	Mild steel	1.0 M HCl	>88	physisorption as well as chemisorption	[12]
1-Phenyl-3-Amino-5-Pyrazolone	Mild steel	0.5 M H_2SO_4	98	physisorption as well as chemisorption	[29]
Halogen-substituted pyrazolo-pyrimidine derivatives: 3-methyl-6-oxo-4,5,6,7-tetrahydro-2H-pyrazolo[3,4-b]pyridine-5--carbonitrile (APP I), 3-methyl-6-oxo-4-(3-phenoxyphenyl)-4,5,6,7-tetrahydro-2H-pyrazolo[3,4-b]pyridine-5-carbonitrile (APP II) and 3-methyl-6-oxo-4-(thiophen-2-yl)--4,5,6,7-	Copper	0.5 M H_2SO_4	>70	Langmuir, chemisorption and physical absorption.	[30]

Inhibitor	Electrode	Medium	IE %	Adsorption isotherm	Ref.
-tetrahydro-2H-pyrazolo[3,4-b]pyridine-5 carbonitrile (APP III)					
Pyrazolone derivative	Mild steel	0.5 M H_2SO_4	91	Langmuir & Temkin, physical adsorption	[31]
pyrazolone derivatives: 4-(2-(4-(N-(pyrimidin-2-yl)sulfamoyl) phenyl)hydrazono)-3-methyl-1-thiocarbamoyl-2-pyrazolin-5--one(PY1) and (4-methyl-3-phenylthiazol-2-ylidene)-3-methyl--1-thiocarbamoyl-2-pyrazolin-5-one (Py2)	Carbon steel	1.0 M HCl	>80	Temkin isotherm, physical adsorption	[32]
5-Methyl-2,4-dihydropyrazol-3-one and 5-methyl-2-phenyl-2,4-didhydropyrazol-3-one	Copper	0.1 M H_2SO_4	76	Langmuir, physical adsorption	[33]
Imidazole derivatives	Copper	0.5 M H_2SO_4	>9 5	Langmuir, chemisorption and physical adsorption	[34]
Aryl pyrazolo pyridines: 3-methyl-6-oxo-4,5,6,7-tetrahydro--2H-pyrazolo[3,4-b]pyridine-5-carbonitrile (APP I), 3-methyl--6-oxo-4-(3-phenoxyphenyl)-4,5,6,7-tetrahydro-2H-pyrazo-lo[3,4-b]pyridine-5-carbonitrile (APP II) and 3-methyl-6-oxo4--(thiophen-2-yl)-4,5,6,7-tetrahydro-2H-pyrazolo[3,4-b]pyri-dine-5-carbonitrile (APP III)	Copper	0.5 M HCl	92	-	[35]
pyrazolone derivatives: 2-(3-amino-5-oxo-4,5-dihydro-1*H*--pyrazol-1-yl)(*p*-tolyl)methyl)malononitrile (PZ-1) and 2-((3--amino-5-oxo-4,5-dihydro-1*H*-pyrazol-1-yl)(phenyl)meth-yl)malononitrile (PZ-2)	N80 Steel	15 % HCl	>90	-	[36]
Pyrazolo-pyrimidine derivatives	Copper	0.5 M H_2SO_4	>70 %	-	[37]
H, 4H, 5H-pyrazolo[3,4-d]pyrimidine	Copper	synthetic seawater	>90	Langmuir, chemisorption	[38]
5-methyl, 5-phenyl, and 5-methyl-2-phenyl derivatives of 2,4-dihydro-3H-pyrazol-3-one (Py)	Copper	H_2SO_4	>84	Langmuir, physical adsorption	This work

Adsorption isotherm

To fit the adsorption of the used additives, we tried to estimate the perfect adsorption isotherm realized our obtained results. Among the isotherms, Langmuir, Frumkin, Temkin, Freundlich, and Florry-Huggins, were checked using the degree of surface covering (θ) calculated from weight loss measurements. The experimental data showed that the Langmuir adsorption isotherm provided the most accurate description of adsorption of pyrazolone compounds on the copper surface. The Langmuir-isotherm can be expressed according to the Equation (27) and its logarithmic form, given by Equation (28) [39]:

$$c/\theta = 1/K + \mathrm{c} \quad (27)$$

where K is the adsorption equilibrium constant, θ is the degree of inhibitor's surface covering, and C is the inhibitor concentration in the bulk electrolyte.

$$\log (c/\theta) = \log c - \log K \quad (28)$$

The Langmuir adsorption isotherm is the perfect one that fits the results of adsorption of pyrazolone derivatives on the surface of copper as detected from the linear relationship between log (c/θ) and log c plots, shown in Figure 11.

From the intercepts of the straight lines of Figure 11, the equilibrium constant (K) values could be calculated. In the same way, K values can be calculated for the adsorption process of each pyrazolone compound at different temperatures (Table 5). Examination of data of Figure 11 reveals that K value declines in the following order at the test temperature: Py I > Py III > Py II. This could be attributed to the deceased tendency of adsorption of these additives. However, as the temperature is raised, the values of K decrease due to desorption of the inhibitors on rising the temperature [40].

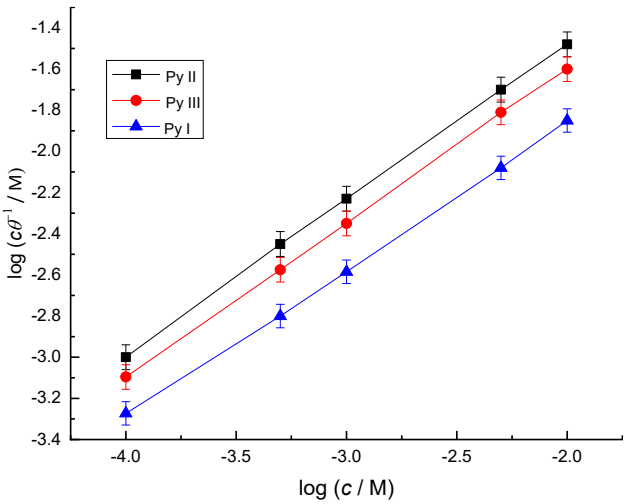

Figure 11. *Plots of log (c/θ)* vs. *log* c*, following 10 h immersion of copper in 0.5 M H_2SO_4 solution at 25 °C*

The equilibrium constant of adsorption, *K*, is related to the free energy of adsorption (ΔG_{ads}) according to the Equation (29) [39]:

$$\Delta G^{o}_{ads} = -2.303\ RT \log (55.5\ K) \quad (29)$$

The calculated ΔG^{o}_{ads} values were found to be negative and less than -40.0 kJ mol^{-1} indicating that, although pyrazolone derivatives are physically and spontaneously adsorbed on the Cu-surface, the process is less favorable at high temperatures [41]. Equation (30) can also be used to compute the other thermodynamic functions [39]:

$$\Delta G^{o}_{ads} = \Delta H^{o}_{ads} - T\Delta S^{o}_{ads} \quad (30)$$

where, ΔS^{o}_{ads} and ΔH^{o}_{ads} represent the entropy and enthalpy of the process, respectively.

Plotting the computed free energy values (ΔG^{o}_{ads}) for the pyrazolone compounds utilized versus temperature (*T*) yielded straight lines, as illustrated in Figure 12.

Further inspection of the data of Table 5, the values of ΔS^{o}_{ads} for Py I are greater and more negative than those for the other pyrazolone compounds at the same temperature. This indicates an increased propensity for the inhibitory species to adsorb on the metal surface.

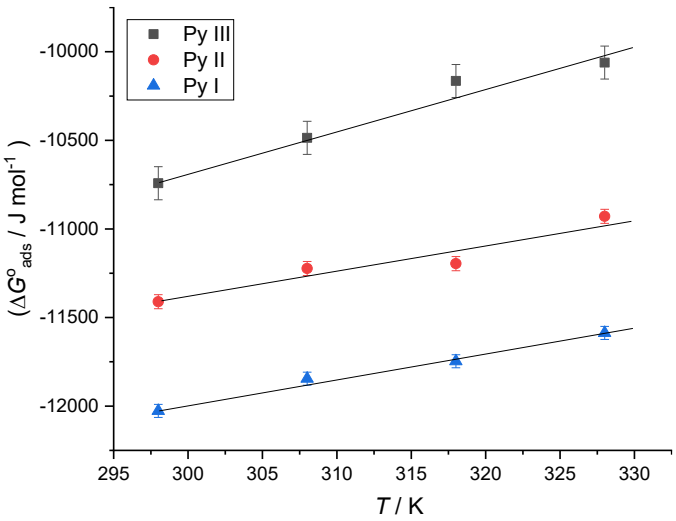

Figure 12. *Temperature dependency of ΔG^{o}_{ads} in 0.5 M H_2SO_4 containing 10 mM of pyrazolone derivatives*

Table 5 includes the values of ΔH^{o}_{ads} in the temperature range of 298 to 328 K for different pyrazolone derivatives. The exothermic nature of the adsorption of these additives on the Cu

surface is shown in the all-negative values of ΔH^{o}_{ads} [41]. In comparison with the other two pyrazolone derivatives, Py II and Py III exhibit less negative ΔH^{o}_{ads}. This suggests even more that Py I adsorbs less on the copper surface than the other two pyrazolone derivatives.

Table 5. *Values of* K, ΔG^{o}_{ads}, ΔH^{o}_{ads} *and* ΔS^{o}_{ads} *for adsorption of pyrazolone derivatives on the copper surface at different temperatures (298 to 328 K)*

Inhibitor	Parameter	Temperature, K			
		298	308	318	328
Py II	K / L mol^{-}	76.33±0.41	60.00±0.52	46.72±0.14	40.00±0.67
	$-\Delta G^{o}_{ads}$ / kJ mol^{-1}	10.74±0.06	10.49±0.18	10.17±0.00	10.06±0.05
	$-\Delta H^{o}_{ads}$ / kJ mol^{-1}	15.80±0.10			
	$-\Delta S^{o}_{ads}$ / J mol^{-1}	16.97±0.49	17.25±0.16	17.72±0.32	16.98±0.51
Py III	K / L mol^{-1}	100.00±0.77	80.00±0.28	69.00±0.53	55.00±0.60
	$-G^{o}_{ads}$ / kJ mol^{-1}	11.41±0.31	11.22±0.13	11.196±0.09	10.93±0.25
	$-\Delta H^{o}_{ads}$ / kJ mol^{-1}	15.8±0.10			
	$-\Delta S^{o}_{ads}$ / J mol^{-1}	16.97±0.49	16.97±0.49	16.97±0.50	16.97±0.49
Py I	K / L mol^{-1}	128.20±0.81	102.20±0.54	85.00±0.09	70.00±0.11
	$-\Delta G^{o}_{ads}$ / kJ mol^{-1}	12.03± 0.56	11.85±0.57	11.75± 0.53	11.59±0.30
	$-\Delta H^{o}_{ads}$ / kJ mol^{-1}	17.76± 0.61			
	$-\Delta S^{o}_{ads}$ / J mol^{-1}	19.23± 0.44	19.20±0.31	18.90±0.28	18.82±0.34

Computational study

Optimizing geometry for pyrazolone derivatives

All quantum chemical data have been extracted by implementing geometric optimization concerning all nuclear coordinates using DFT based on the 6-31G basis set and B3LYP method as the level of theory. The optimal configuration of the examined chemical as well as their molecular electrostatic potential surface (MESP) is depicted in Figure 13.

Different colors clarify the electrostatic potential at various locations on the electron density surfaces. Electrophilic active areas, which have the highest negative electrostatic potential, are characterized by their red hue. Whereas the green color denotes a region of zero potential, the blue hue indicates the regions with the highest electrostatic potential (nucleophilic region). The possibility increases in the order green < blue < yellow < orange < red [42].

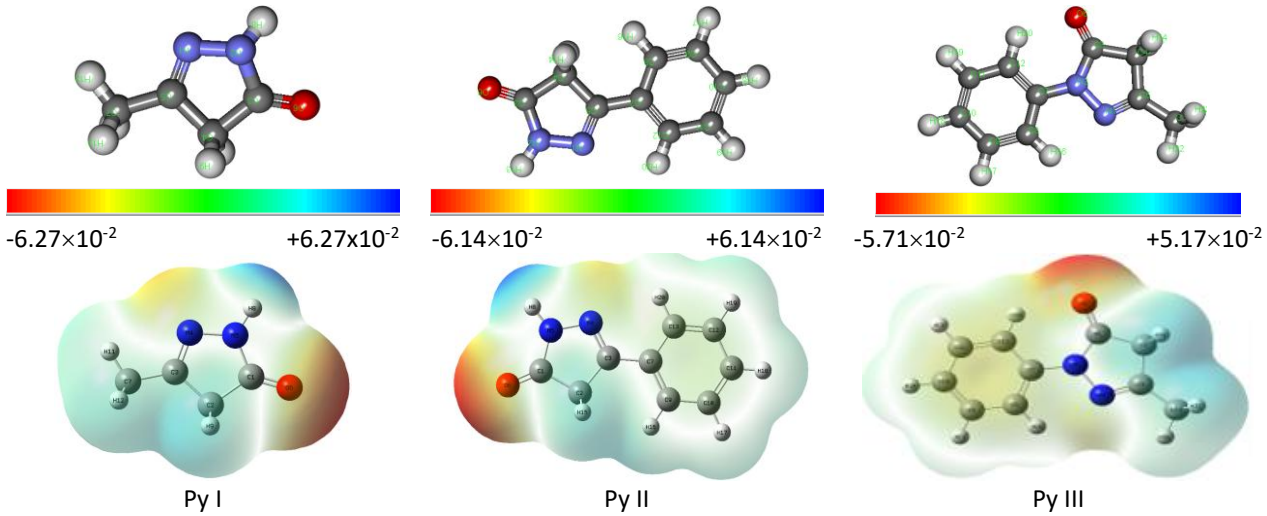

Figure 13. *The optimized structures and electrostatics of examined pyrazolone molecules*

Figure 13 displays the three compounds' electrostatic potential. Heteroatoms and conjugated double bonds are the main locations of the electron-rich areas. Negative areas that are conducive to electrophilic assaults are indicated by the N, NH, O and pyrazolone rings. Blue (positive sign) hydrogen atoms are more likely to be attacked by nucleophiles. The HOMO density location in the pyrazolone derivatives is mostly distributed near the nitrogen (*i.e.* NH or N), oxygen (=O) atoms, and pyrazolone rings, indicating that these are the preferred sites for adsorption [43], which is confirmed by both Mulliken negative charges and largest Fukui positive f_k^+ and f_k^- values for all inhibitors, whereas the LUMO density was distributed almost throughout the molecules. Table 6 shows the calculated DFT parameters of the examined compounds, where data show that, in the gas phase, PYI and PYI H+ show balanced stability and reactivity with moderate $\Delta E_{(H-L)}$ values (5.787 and 6.153 eV). PY II exhibits the strongest reactivity with the smallest $\Delta E_{(H-L)}$ value (4.586 eV) and the highest electronegativity (4.395 eV). PY III shows balanced stability and reactivity with a moderate gap (4.829 eV) and the highest ΔN value (0.191), indicating greater electron transport.

In the water phase, PYI and PYI H+ show balanced stability and reactivity with moderate ΔE values (5.872 and 6.366 eV). PY II has the smallest ΔE_{gap} (5.998 eV) and the highest electronegativity (6.787 eV), indicating strong electron-accepting capacity. PY III exhibits balanced stability and reactivity with a moderate ΔE_{gap} (5.059 eV) and the highest ΔN value (0.165), indicating greater electron transport.

Table 6. *Calculated quantum chemical parameters of examined pyrazolone compounds*

	E_{HOMO} / eV	E_{LUMO}/ eV	ΔE_g / eV	I / eV	A / eV	X / eV	H / eV	π /eV	σ / eV^{-1}	ω / eV	ω+ / eV	ω- / eV	$\Delta\omega$+ / eV	ΔN	$\Delta E_{back\ donation}$ / eV
Gaseous state															
PYI	-6.706	-0.919	5.787	6.706	0.919	3.812	2.893	-3.812	0.3456	2.511	0.967	4.779	5.746	0.107	0.723
PYI H+	-7.007	-0.853	6.153	7.006	0.853	3.930	3.077	-3.930	0.325	2.510	0.9297	4.859	5.789	0.081	0.769
PYII	-6.275	-1.688	4.586	6.274	1.688	3.981	2.293	-3.981	0.436	3.456	1.7527	5.733	7.486	0.098	0.573
PYII H+	-7.103	-1.688	5.414	7.103	1.688	4.395	2.707	-4.395	0.369	3.568	1.709	6.104	7.813	0.006	0.677
PYIII	-5.922	-1.094	4.829	5.922	1.094	3.508	2.414	-3.508	0.414	2.549	1.100	4.604	5.701	0.191	0.604
PYIII H+	-6.805	-1.140	5.665	6.805	1.140	3.972	2.832	-3.972	0.353	2.785	1.153	5.126	6.279	0.081	0.708
Liquid (water)															
PYI	-6.746	-0.873	5.872	6.745	0.873	3.809	2.936	-3.809	0.341	2.471	0.933	4.742	5.675	0.106	0.734
PYI H+	-7.167	-0.801	6.367	7.167	0.801	3.984	3.183	-3.984	0.314	2.493	0.899	4.883	5.782	0.070	0.796
PYII	-8.934	-2.372	6.561	8.933	2.372	5.653	3.280	-5.653	0.305	4.871	2.454	8.107	10.560	-0.186	0.820
PYII H+	-9.787	-3.788	5.998	9.786	3.788	6.787	2.999	-6.787	0.333	7.681	4.662	11.449	16.111	-0.393	0.750
PYIII	-6.124	-1.064	5.059	6.124	1.064	3.594	2.530	-3.594	0.395	2.553	1.072	4.667	5.739	0.165	0.632
PYIII H+	-7.091	-0.485	6.606	7.091	0.485	3.788	3.303	-3.788	0.303	2.172	0.691	4.479	5.170	0.097	0.826

The obtained adsorption data of the three pyrazolone derivatives and the $Cu_{(111)}$ surface are tabulated in Table 7. The three molecules were adsorbed on a parallel position to the $Cu_{(111)}$ surface. The plane position leads to the maximum interaction between the active sites of the organic inhibitors and the metal surface [44] as shown in Figure 14.

Table 7*. Lower adsorption configuration output results from the adsorption locator module*

	Energy, kJ mol^{-1}				(dE_{ads}/dN_i) / kJ mol^{-1}
Structures	Total	Adsorption	Rigid adsorption	Deformation	
Cu_{111}+PYI+ 98H_2O+ 2H_2SO_4	-351.92	-238.756	-196.933	-41.8233	-238.756
Cu_{111}+PYII+ 98H_2O+ 2H_2SO_4	-191.058	-190.272	-151.406	-38.8652	-190.272
Cu_{111}+PYIII+ 98H_2O+ 2H_2SO_4	-370.468	-318.097	-290.081	-28.0202	-318.097

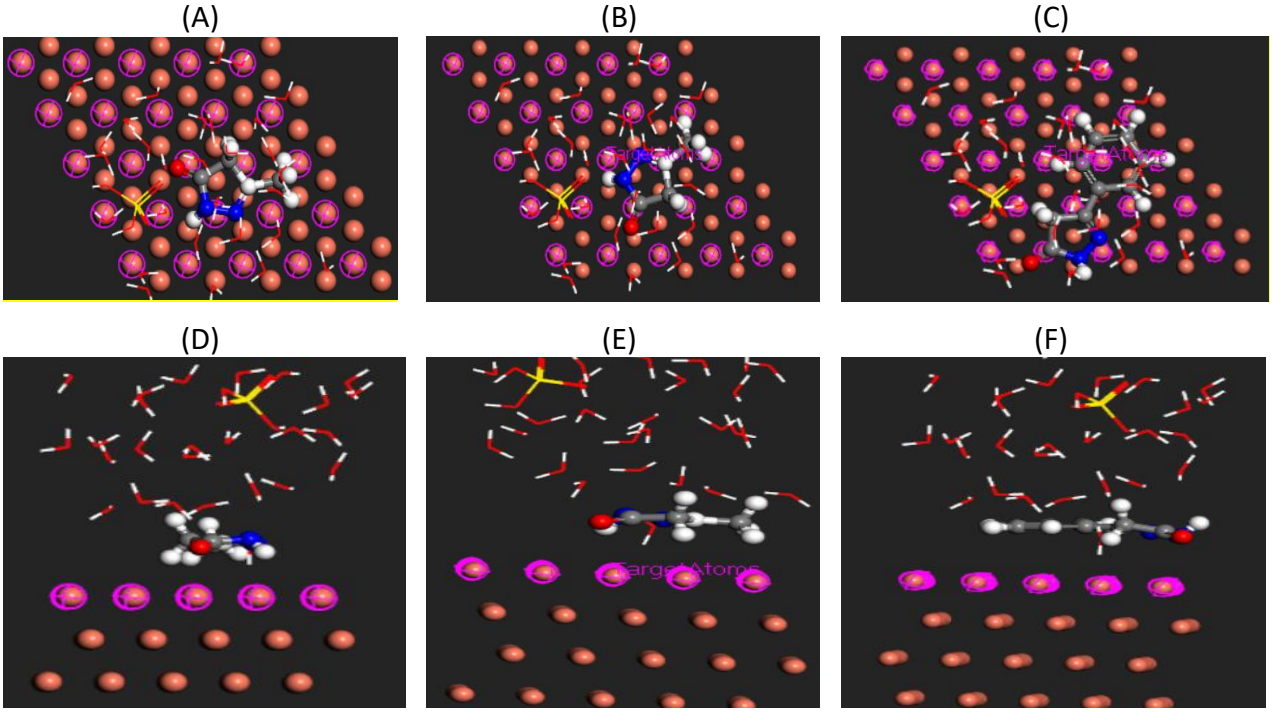

Figure 14. *Side and top views of most stable adsorption configuration of Py I (A) and (D), Py II (B) and (E) and Py III (C) and (F) obtained by molecular dynamic simulations on Cu_{111}/98 H_2O/2H_2SO_4 surface*

Inhibitory mechanism

At least one polar unit, comprising atoms of N, O, S and, in certain situations Se and P, is required for the majority of organic compounds that can be employed as inhibitors. These kinds of substances are capable of donating electrons, and their mechanism of action is thought to be due to the adsorption of inhibitor molecules onto the surfaces of metals via an unshared pair of heteroatom electrons [45].

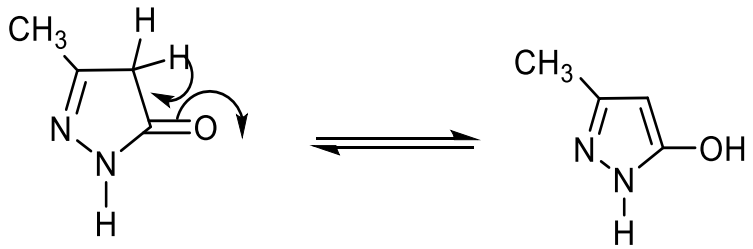

Figure 15. *The keto-enol forms of Py I*

Figure 15 shows the equilibrium of the keto and enol forms of Py I in an acidic medium. It is suggested that the interaction of the lone pair of electrons from the O-atom of the keto-enol, with the positively charged metal surface is the cause of the inhibition of Cu in an acidic medium. Other factors that must be taken into account in the corrosion inhibition process include the interaction of the electrons from the pyrazolone rings with the positively charged metal surface and the interaction of pyrazolone cations formed in acidic solutions with the negatively charged metal surface. Conversely, inhibitors' delocalized π -electrons enable high adsorption on the Cu-surface, which causes inhibition of corrosion [46]. Two factors may be responsible for Py I maximum inhibitory action: (i) the smallest molecule size; and (ii) the existence of an electron-donating group (-CH_3) that raised the pyrazolone ring electron density. These factors led to an increase in the adsorption process. The review of the literature also shows that pyrazolone derivatives are good corrosion inhibitors, particularly in acidic media, because of their strong adsorption through the

donation of O and N atoms' lone pairs of electrons to the metal surface [46] which is corroborated by Mulliken charges and Fukui indices.

SEM micrographs of the copper electrode surface taken before, after 10-hour immersion in 0.5 M sulfuric acid (free) and 0.5 M sulfuric acid with 10 mM Py I (an example of the utilized inhibitor) are shown in Figure 16. Examining these micrographs reveals that in H_2SO_4 free solution, the formation of little pits, some of which equally grew inward and laterally to produce some sizable attacked areas (compared by the Cu-surface before immersion in H_2SO_4 (Figure 16(A)). Traces of the corrosion products are seen inside these sizable regions, as shown in Figure 16(B). However, the number and size of pits created are significantly reduced in the presence of 10 mM Py I , as an example of organic inhibitors utilized (Figure 16(C)).

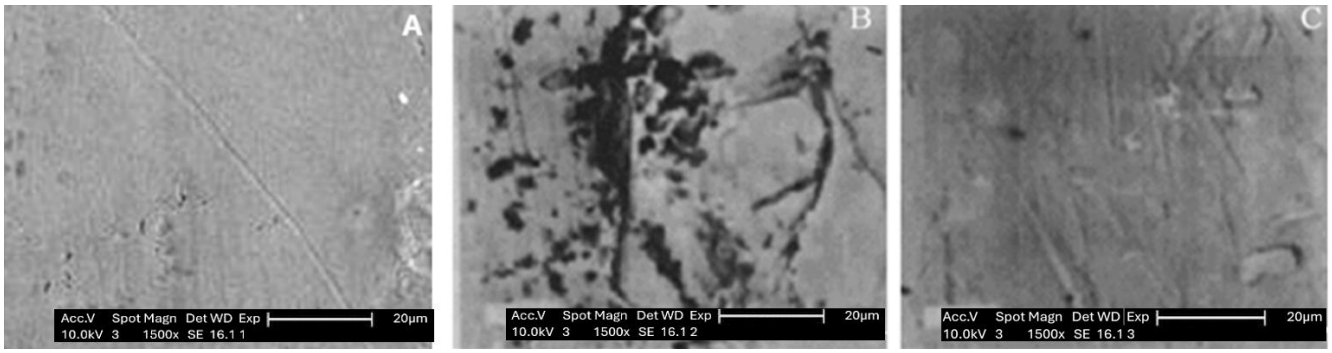

Figure 16. *SEM micrographs of copper electrode surface: (A) after immersion for a period of 10 h in (B) 0.5 M sulfuric acid (free) and (C) 0.5 M sulfuric acid + 10 mM Py I.*

Conclusions

The results of the present demonstrated the following:

Higher acid concentrations and longer exposure times cause copper to corrode more quickly in H_2SO_4 solutions. Weight loss and polarization measurements show that corrosion rates rise as temperature and acid concentration rise. The rates of copper corrosion in sulfuric acid are decreased by pyrazolone derivatives, and the efficiency of inhibition increases with increasing inhibitor concentration. The order of inhibitory efficiency at the same temperature is as follows: Py I < Py II < Py III. SEM demonstrates that these compounds significantly reduce corrosion regions. Quantum generally support lab results, strengthening the use of pyrazolone as a corrosion inhibitor for Cu in H_2SO_4.

Declaration of competing Interest: *The authors declare that they have no known competing financial interests or personal relationships that could have appeared to influence the work reported in this paper.*

Acknowledgments: *Authors are thankful to the Department of Chemistry, Faculty of Science, Zagazig University, Zagazig for providing laboratory facilities.*

References

[1] L. Nunez, E. Reguera, F. Corvo, E. González, C. Vazquez, Corrosion of copper in seawater and its aerosols in a tropical island, *Corrosion Science* **47** (2005) 461-484. https://doi.org/10.1016/j.corsci.2004.05.015

[2] A.-Y. Zhu, J.-l. Chen, L. Zhou, L.-y. Luo, Q. Lei, L. Zhang, W. Zhang, Hot deformation behavior of novel imitation-gold copper alloy, *Transactions of Nonferrous Metals Society of China* **23** (2013) 1349-1355. https://doi.org/10.1016/S1003-6326(13)62603-5

[3] E. T. Akinlabi, A. Andrews, S. A. Akinlabi, Effects of processing parameters on corrosion properties of dissimilar friction stir welds of aluminium and copper, T*ransactions of*

Nonferrous Metals Society of China **24** (2014) 1323-1330. https://doi.org/10.1016/S1003-6326(14)63195-2

[4] B. Tan, S. Zhang, Y. Qiang, W. Li, H. Liu, C. Xu, S. Chen, Insight into the corrosion inhibition of copper in sulfuric acid via two environmentally friendly food spices: Combining experimental and theoretical methods, *Journal of Molecular Liquids* **286** (2019) 110891. https://doi.org/10.1016/j.molliq.2019.110891

[5] A. Zarrouk, B. Hammouti, A. Dafali, F. Bentiss, Inhibitive properties and adsorption of purpald as a corrosion inhibitor for copper in nitric acid medium, *Industrial & Engineering Chemistry Research* **52** (2013) 2560-2568. https://doi.org/10.1021/ie301465k

[6] R. Chadli, M. Elazouzi, I. Khellad, A. M. Elhourri, H. Elmsellem, A. Aouniti, J. K. Mulengi, B. Hammoutii, Electrochemical and theoretical study of pyrazole 4-(4,5-dihydro-1H-pyrazol-5-yl)-N,N-dimethylaniline (D) as a corrosion inhibitor for mild steel in 1 M HCl, Portugaliae *Electrochimica Acta* **35** (2017) 65-80. https://doi.org/10.4152/pea.201702065

[7] K.-c. Shen, G.-h. Li, W.-m. Wang, Thermal expansion behavior, microhardness and electrochemical corrosion resistance properties of $Au_{52}Cu_{27}Ag_{17-x}(NiZn0.5)_x$ alloys, *Transactions of Nonferrous Metals Society of China* **26** (2016) 2900-2909. https://doi.org/10.1016/S1003-6326(16)64419-9

[8] M. Akrom, S. Rustad, A. G. Saputro, H. K. Dipojono, Data-driven investigation to model the corrosion inhibition efficiency of pyrimidine-pyrazole hybrid corrosion inhibitors, *Computational and Theoretical Chemistry* **1229** (2023) 114307. https://doi.org/10.1016/j.comptc.2023.114307

[9] H. Chahmout, M. Ouakki, S. Sibous, M. Galai, N. Arrousse, E. Ech-chihbi, Z. Benzekri, S. Boukhris, A. Souizi, M. Cherkaoui, New pyrazole compounds as a corrosion inhibitor of stainless steel in 2.0 M H_2SO_4 medium: Electrochemical and theoretical insights, *Inorganic Chemistry Communications* **147** (2023) 110150. https://doi.org/10.1016/j.inoche.2022.110150

[10] S. Abd El Rehim, S. Sayyah, M. El-Deeb, S. M. Kamal, R. E. Azooz, Adsorption and corrosion inhibitive properties of P (2-aminobenzothiazole) on mild steel in hydrochloric acid media, I*nternational Journal of Industrial Chemistry* **7** (2016) 39-52. https://doi.org/10.1007/s40090-015-0065-5

[11] H. Lgaz, R. Salghi, A. Chaouiki, Shubhalaxmi, S. Jodeh, K. S. Bhat, Pyrazoline derivatives as possible corrosion inhibitors for mild steel in acidic media: A combined experimental and theoretical approach, *Cogent Engineering* **5** (2018) 1441585. https://doi.org/10.1080/23311916.2018.1441585

[12] H. Lgaz, S. K. Saha, A. Chaouiki, K. S. Bhat, R. Salghi, Shubhalaxmi, P. Banerjee, I. H. Ali, M. I. Khan, I. M. Chung, Exploring the potential role of pyrazoline derivatives in corrosion inhibition of mild steel in hydrochloric acid solution: Insights from experimental and computational studies, *Construction and Building Materials* **233** (2020) 117320. https://doi.org/10.1016/j.conbuildmat.2019.117320

[13] A. Chaouiki, M. Chafiq, H. Lgaz, H. Shubhalaxmi, K. S. Bhat, I. H. Ali, S. Masroor, Y. El Aoufir, Experimental and theoretical insights into the corrosion inhibition activity of a novel pyrazoline derivative for mild steel in 1.0 M HCl, *Applied Journal of Environmental Engineering Science* **6** (2020) 2079-2093. https://doi.org/10.48422/IMIST.PRSM/ajees-v6i1.20261

[14] N. A. Wazzan, I. Obot, S. Kaya, Theoretical modeling and molecular level insights into the corrosion inhibition activity of 2-amino-1,3,4-thiadiazole and its 5-alkyl derivatives, *Journal of Molecular Liquids* **221** (2016) 579-602. https://doi.org/10.1016/j.molliq.2019.117320

[15] A.-B. Kamal, M. Mostfa, A. M. Ashmawy, M. S. El-Gaby, G. A. Ali, Corrosion inhibition behavior of the synthesized pyrazoline-sulfonamide hybrid of mild steel in aqueous

solutions: Experimental and quantum investigations, J*ournal of Chemical Sciences* **134** (2022) 90. https://doi.org/10.1007/s12039-022-02086-6

[16] R. G. Pearson, Absolute electronegativity and hardness: applications to organic chemistry, *The Journal of Organic Chemistry* **54** (1989) 1423-1430. https://doi.org/10.1021/jo00267a034

[17] S. Martinez, Inhibitory mechanism of mimosa tannin using molecular modeling and substitutional adsorption isotherms, *Materials Chemistry and Physics* **77** (2003) 97-102. https://doi.org/10.1016/S0254-0584(01)00569-7

[18] R. G. Parr, L. V. Szentpály, S. Liu, Electrophilicity index, J*ournal of the American Chemical Society* **121** (1999) 1922-1924. https://doi.org/10.1021/ja983494x

[19] W. Yang, W. J. Mortier, The use of global and local molecular parameters for the analysis of the gas-phase basicity of amines, *Journal of the American Chemical Society* **108** (1986) 5708-5711. https://doi.org/10.1021/ja00279a008

[20] C. Morell, A. Grand, A. Toro-Labbé, Theoretical support for using the Δf (r) descriptor, *Chemical Physics Letters* **425** (2006) 342-346. https://doi.org/10.1016/j.cplett.2006.05

[21] Z. Qu, X. Wang, X. Shen, H. Zhou, Study of the Cu (111) Surface by Scanning Tunneling Microscopy: The Morphology Evolution, Reconstructions, Superstructures and Line Defects, *Nanomaterials* **12** (2022) 4278. https://doi.org/10.3390/nano12234278

[22] M. Iwai, H. Majima, Y. Awakura, Dissolution of copper in hydrochloric acid solutions with dissolved molecular oxygen, *Hydrometallurgy* **20** (1988) 87-95. https://doi.org/10.1016/0304-386X(88)90028-X

[23] M. Braun, K. Nobe, Electrodissolution kinetics of copper in acidic chloride solutions, *Journal of The Electrochemical Society* **126** (1979) 1666. https://iopscience.iop.org/article/10.1149/1.2128773/meta

[24] L. Gao, S. Peng, X. Huang, Z. Gong, A combined experimental and theoretical study of papain as a biological eco-friendly inhibitor for copper corrosion in H_2SO_4 medium, *Applied Surface Science* **511** (2020) 145446. https://doi.org/10.1016/j.apsusc.2020.145446

[25] A. A. Mahmmod, A. A. Khadom, A. A. H. Kadhum, A. Alamiery, Quinoxaline as a corrosion inhibitor for copper in nitric acid: Kinetics, statistical, and theoretical investigations, *Case Studies in Chemical and Environmental Engineering* **10** (2024) 100836. https://doi.org/10.1016/j.cscee.2024.100836

[26] F. R. García-Galvan, S. Fajardo, V. Barranco, S. Feliu Jr, Experimental apparent stern–geary coefficients for AZ31B Mg alloy in physiological body fluids for accurate corrosion rate determination, *Metals* **11** (2021) 391. https://doi.org/10.3390/**met11030391**

[27] C. Jeyaprabha, S. Sathiyanarayanan, K. Phani, G. Venkatachari, Influence of poly (amino-quinone) on corrosion inhibition of iron in acid media, *Applied Surface Science* **252** (2005) 966-975. https://doi.org/10.1016/j.apsusc.2005.01.098

[28] R. T. Loto, C. A. Loto, A. P. Popoola, T. Fedotova, Inhibition effect of 2-amino-5-ethyl-1, 3, 4-thiadiazole on corrosion behaviour of austenitic stainless steel type 304 in dilute HCl solution, *Journal of Central South University* **23** (2016) 258-268. https://doi.org/10.1007/s11771-016-3069-1

[29] Y. Zhang, Y. Cheng, F. Ma, K. Cao, Corrosion inhibition of carbon steel by 1-phenyl-3-amino-5-pyrazolone in H_2SO_4 solution, I*nternational Journal of Electrochemical Science* **14** (2019) 999-1008. https://doi.org/10.20964/2019.01.69

[30] Y. Xu, S. Zhang, C. Liao, Y. Zhou, L.H. Madkour, Halogen-substituted pyrazolo-pyrimidine derivatives as corrosion inhibitors for copper in sulfuric acid solution, *International Journal of Corrosion and Scale Inhibition* **7** (2018) 236-249. https://doi.org/10.17675/2305-6894-2018-7-2-9

[31] D. Nalini, K. Kohilah, R. Sowmya, A combined experimental and theoretical investigation on pyrazolone derivative as corrosion inhibitor for mild steel in 0.5 M sulphuric acid media, *Portugaliae Electrochimica Acta* **32** (2014) 109-123. https://doi.org/10.4152/pea.201402109

[32] M. Deyab, A. Fouda, M. Osman, S. Abdel-Fattah, Mitigation of acid corrosion on carbon steel by novel pyrazolone derivatives, *RSC Advances* **7** (2017) 45232-45240. https://doi.org/10.1039/C7RA08761F

[33] A. Díaz-Gómez, R. Vera, A. Molinari, A. Oliva, W. Aperador, 5-Methyl-2, 4-dihydropyrazol-3-one and 5-methyl-2-phenyl-2, 4-didhydropyrazol-3-one as copper corrosion inhibitors in acidic media, *International Journal of Electrochemical Science* **10** (2015) 4004-4019. https://doi.org/10.1016/S1452-3981(23)06597-5

[34] T. Yan, S. Zhang, L. Feng, Q. Yujie, L. Lansi, F. Denglin, W. Yanan, C. Jida, L. Wenpo, T. Bochuan, Investigation of imidazole derivatives as corrosion inhibitors of copper in sulfuric acid: combination of experimental and theoretical researches, *Journal of the Taiwan Institute of Chemical Engineers* **106** (2020) 118-129. https://doi.org/10.1016/j.jtice.2019.10.014

[35] M. Quraishi, The corrosion inhibition effect of aryl pyrazolo pyridines on copper in hydrochloric acid system: computational and electrochemical studies, *RSC Advances* **5** (2015) 41923-41933. https://doi.org/10.1039/C5RA03966E

[36] K. Ansari, M. Quraishi, A. Singh, S. Ramkumar, I. B. Obote, Corrosion inhibition of N80 steel in 15% HCl by pyrazolone derivatives: electrochemical, surface and quantum chemical studies, *RSC Advances* **6** (2016) 24130-24141. https://doi.org/10.1039/C5RA25441H

[37] Y. Xu, S. Zhang, W. Li, L. Guo, S. Xu, L. Feng, L. H. Madkour, Experimental and theoretical investigations of some pyrazolo-pyrimidine derivatives as corrosion inhibitors on copper in sulfuric acid solution, *Applied Surface Science* **459** (2018) 612-620. https://doi.org/10.1016/j.apsusc.2018.08.037

[38] S. Echihi, N. Benzbiria, M. Belghiti, M. El Fal, M. Boudalia, E. M. Essassi, A. Guenbour, A. Bellaouchou, M. Tabyaoui, M. Azzi, Corrosion inhibition of copper by pyrazole pyrimidine derivative in synthetic seawater: experimental and theoretical studies, *Materials Today: Proceedings* **37** (2021) 3958-3966. https://doi.org/10.1016/j.matpr.2020.09.264

[39] S. Abd El Rehim, S. Sayyah, M. El-Deeb, S.M. Kamal, R. E. Azooz, Poly (o-phenylenediamine) as an inhibitor of mild steel corrosion in HCl solution, *Materials Chemistry and Physics* **123** (2010) 20-27. https://doi.org/10.1016/j.matchemphys.2010.02.069

[40] R. Zvauya, J. Dawson, Inhibition studies in sweet corrosion systems by a quaternary ammonium compound, J*ournal of Applied Electrochemistry* **24** (1994) 943-947. https://doi.org/10.1007/BF00348786

[41] P. Desai, R. Vashi, Inhibitive efficiency of sulphathiazole for aluminum corrosion in trichloroacetic acid, *Anti-Corrosion Methods and Materials* **58** (2011) 70-75. https://doi.org/10.1108/00035591111110714

[42] S. S. Pingale, A. P. Ware, S. R. Gadre, Unveiling electrostatic portraits of quinones in reduction and protonation states, *Journal of Chemical Sciences* **130** (2018) 50. https://doi.org/10.1007/s12039-018-1450-3

[43] M. Mostfa, H. Gomaa, I. M. Othman, G. A. Ali, Experimental and theoretical studies of a novel synthesized azopyrazole-benzenesulfonamide derivative as an efficient corrosion inhibitor for mild steel, *Journal of the Iranian Chemical Society* **18** (2021) 1231-1241. https://doi.org/10.1007/s13738-020-02106-7

[44] Y. Boughoues, M. Benamira, L. Messaadia, N. Ribouh, Adsorption and corrosion inhibition performance of some environmental friendly organic inhibitors for mild steel in HCl solution via experimental and theoretical study, *Colloids and Surfaces A: Physicochemical*

and Engineering Aspects **593** (2020) 124610. https://doi.org/10.1016/j.colsurfa.2020.124610

[45] L. Herrag, A. Chetouani, S. Elkadiri, B. Hammouti, A. Aouniti, Pyrazole derivatives as corrosion inhibitors for steel in hydrochloric acid, *Portugaliae Electrochimica Acta* **26** (2008) 211-220. https://peacta.org/articles_upload/PEA_26_2_211_220.pdf

[46] A. Zarrouk, B. Hammouti, A. Dafali, Inhibition of copper corrosion in acid solution by N-1-naphthylethylenediamine dihydrochloride monomethanolate: experimental and theoretical study: part-1, *Research on Chemical Intermediates* **38** (2012) 1079-1089. https://doi.org/10.1007/s11164-011-0444-2